CFD and Kinetic Methods for Mass Transfer Determination in a Mesh Microreactor

Radwan Abdallah, Pierre Magnico, Bruno Fumey, and Claude de Bellefon
Laboratoire de Génie des Procédés Catalytiques, CNRS-ESCPE Lyon, BP2077, 69616 Villeurbanne, France

DOI 10.1002/aic.10822
Published online April 11, 2006 in Wiley InterScience (www.interscience.wiley.com).

The global gas-liquid-solid volumetric mass-transfer coefficient $K_L a$ *of a catalytic multiphase microstructured film contactor, featuring 5 μm dimensions, a 155 μm liquid film thickness, and a 15 μm thin catalytic layer is determined, using the very fast hydrogenation of α-methylstyrene with a Pd/γ-alumina catalyst. The volumetric mass-transfer coefficients measured experimentally fall in the range 0.8 – 1.6* s^{-1} *above that predicted by the film model and those obtained from a CFD (3-D model) simulation, and from an analytical solution.* © 2006 American Institute of Chemical Engineers *AIChE J,* 52: 2230–2237, 2006

Keywords: mass transfer, catalysis, gas-liquid-solid, microstructured reactor, CFD, hydrogenation

Introduction

Microstructured reactors have attracted considerable attention for various applications in recent years.[1-3] These microdevices are characterized by a laminar flow and very high-surface to volume ratio, which leads to the increase of mass and heat transfer, and offers the potential for process intensification. The very small material inventory when using these microdevices is another advantage for use in high throughput experimentation for lead discovery, and kinetic investigation at reduced costs.[2,4-6]

Hydrodynamics and mass-transfer characterization of these microdevices is mandatory when quantitative studies, such as kinetic investigation are targeted. Mass transfer may be characterized by physical and chemical methods, or estimated using computational fluid dynamics (CFD).

CFD is extensively used for catalytic structured reactor to analyze the velocity field and the mixing process at the local level.[7-9] However, few examples lead to the characterization at the global scale and to the determination of mass-transfer correlations. For example, the mass-transfer coefficients in washcoated monoliths for various geometric shapes, and the dependency of the Sherwood number on the washcoat geometry was investigated and compared with those obtained from an analytical method.[10] The comparison between CFD and published experimental data for Taylor flow regime in capillaries was also investigated.[11] The influence of channel geometry and fluid velocity on a gas-liquid catalytic reaction in a flat plate microreactor was investigated using CFD.[12] In recent work, solid-liquid mass transfer in fixed-bed catalytic reactors has been studied by means of CFD used at the pore level in two-ordered sphere packings (fcc and bcc). The discrepancy between the simulations and published experimental data was attributed to the packing structure assumption in the CFD simulation.[13] However, to the best of our knowledge, no comparison between experimental and CFD investigation of mass transfer in multiphase catalytic microstructured reactors have been reported so far.

Three main principles may be used for catalytic gas-liquid-solid or gas-liquid reactions: (1) Dispersion of liquid droplets into a continuous gas phase: while, circulation of liquid droplets in an open air atmosphere has been reported in microfluidic systems,[14] no demonstration of this principle for catalysis in microstructured reactors has been published yet, (2) dispersion of a gas in a liquid continuous phase: this principle has been used in a microbubble column,[15-17] and for the generation of microbubbles with an interdigitated micromixer,[6] and (3) contacting a liquid film with a gas phase, either with gravity driven liquid flow, such as in the falling film microreactor (FFMR) from IMM,[15,18,19] or with pressure driven horizontal gas-liquid film contactors,[4,20-22] and in a microstructured packed-bed re-

Correspondence concerning this article should be addressed to C. de Bellefon at cdb@lgbcpe.fr.

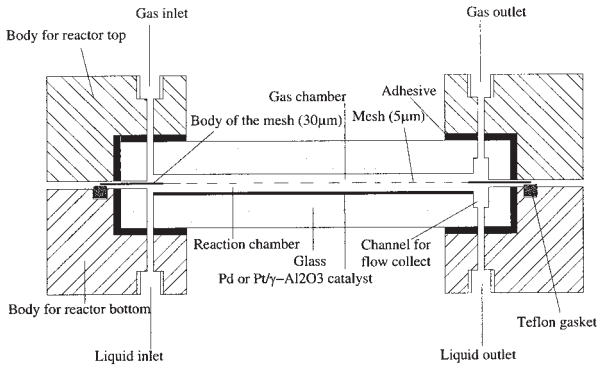

Figure 1. Cross-section of the mesh microcontactor.

actor.[23] These reactors are generally constituted of several parallel reaction channels fed by microstructured gas and liquid distributors generating either microbubbles or fluid sheets. The typical classes of reaction used to characterize the performance of the reactors are chlorination, hydrogenation and direct fluorination.[24] These three classes have been chosen owing to their high exothermicity, the corrosive nature of the gases, and the toxicity of the products, and also the fast reaction rate exhibited.

These microreactors allow to increase the specific gas-liquid interfacial area, in the range 2,000–30,000 m^2/m_L^3, compared to conventional equipment which results in high values of the global mass-transfer coefficient ranging from 1 to 15 s^{-1}. Both the mass-transfer coefficient and the interfacial area depend obviously on the microreactor interface geometry, but also on the flow pattern. In the case of the microbubble column and the packed-bed microreactor, the liquid/gas interface is not stable and several flow patterns have been observed depending on the liquid to gas flow rate ratio. Moreover, in these devices, the gas-liquid feed is not homogeneous and induces several simultaneous flow patterns similar to those observed in capillaries, such as Taylor flow, annular flow and so on. This induces a decrease of the interfacial areas and/or the liquid film thickness, and might also impact the conversion.

In the case of the falling film, visualization experiments showed a stable gas-liquid interface, and a much better homogeneous liquid feed over all the reaction channels (from 32 to 64).[25] The flow stability induces a very narrow residence-time distribution. Two other advantages of the falling film are the possibility to impose a co-current or a counter-current gas flow, and to separate the phases in the reaction volume. However, the range of the liquid flow rate is small owing to the gravity effect, which induces a dependence of the film thickness toward the imposed liquid flow rate.

In this work, a microreactor is used where a metallic mesh insures the gas-liquid interface stability for a large range of the fluid flow rate and, therefore, a laminar flow pattern. This microdevice presents most of the advantages of the falling film microreactor, and, moreover, the volume of reaction does not depend on the flow rate. On the other hand, the interface area, of ca. 2,000 m^2/m_L^3, is smaller than in other microreactors. The mass-transfer characteristics of this "mesh contactor" were investigated by means of the gas-liquid oxidation of alkaline pyrogallol, but without quantitative results.[20] In a preliminary report, the global gas-liquid-solid mass-transfer capability of the "mesh" microcontactor was estimated by means of the fast gas-liquid-solid reaction of hydrogenation of α-methylstyrene into cumene catalyzed by a Pd/$\gamma-Al_2O_3$ catalyst.[4] In this article, the characterization is substantiated by more experimental data and by deeper investigations using the commercial CFD package fluent in the case of a 2-D and 3-D computations, which are compared to an analytical solution.

Reactor description and experimental setup

The description of the mesh reactor has been published.[4,20] It consists of two-phase microreactor that keeps the phases separated. These cavities are separated by a microstructured mesh. The two fluids are in contact through 5 μm dia. holes micromachined in the mesh (Figure 1). The open area between the two phases represents 25% of the total surface of the mesh which leads to an interfacial surface ($a_{G\text{-}L}$) of 1,670 m^2/m_L^3.

The setup used to carry out the experiment is presented in Figure 2. A layer of alumina (γ-Al_2O_3) is deposited on the glass insert of the bottom cavity by wash-coating (density of alumina particle $\rho_p = 10^6$ $g.m^{-3}$ (in agreement with internal porosity of 0.6). The mean thickness of the film catalyst (L) is 15 μm. The content of metals (palladium and platinum) on alumina are 1% wt Pd/γ-Al_2O_3 and 0,9 or 3.6% wt Pt/γ-Al_2O_3. After catalyst coating, the geometrical volume left for the liquid phase is 123 μl with a geometrical liquid film thickness of 155 μm. The α-methylstyrene (AMS) (Aldrich 99%) used contains 15 p.p.m. tert-butylcatechol (a polymerization inhibitor), methylcyclohexane is used as solvent (Aldrich or Acros, 99%). Molecular sieve is added to tank "A". A solution of AMS in methylcyclohexane (3.3 $kmol.m_L^{-3}$) is used for the catalytic tests, either in the pulse (100 μl injected) or continuous modes. The liquid flow is set to 1.67. 10^{-9} $m^3.s^{-1}$, unless otherwise stated and the hydrogen gas flow is of 20 $sccm.h^{-1}$. The temperature and pressure range used for the experiments are 298 – 313 K and 0.2 – 0.5 Mpa, respectively. The liquid collected at the outlet of the reactor (collect time = 12 min for the pulse mode to ensure total recovery of the all material) is analyzed by gas chromatography.

The rate law for the intrinsic activity $a_c(C_s)$, for the used reaction, was established in a previous publication (Eq. 1)[26]

$$a_c(\text{mol}\cdot g_{Pd}^{-1}\cdot s^{-1}) = k_0 \exp\left(-\frac{E_a}{RT}\right)\frac{K_H C_H}{(1+\sqrt{K_H C_H})^2} \qquad (1)$$

with k_0 ($mol.s^{-1}.g_{Pd}{}^{-1}$) =2.17. 10^7; K_H ($m^3.mol^{-1}$) = 1.4. 10^{-2} and E_a ($kJ.mol^{-1}$) = 38.7. The intrinsic rate of reaction per unit

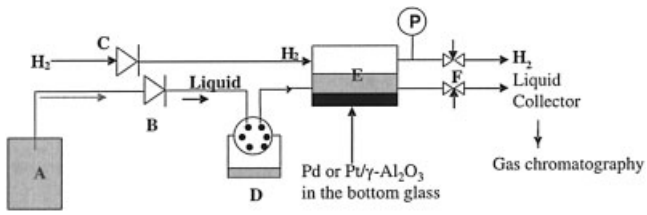

Figure 2. Experimental setup.

(a) Liquid reservoir (methylcyclohexane on molecular sieve); (b) HPLC pump; (c) gas mass-flow meter; (d) valve equipped with a injection loop (100 μl), (E) microreactor; and (f) needle valve; P: pressure gauge. Catalyst: Pd or Pt/ γ-alumina.

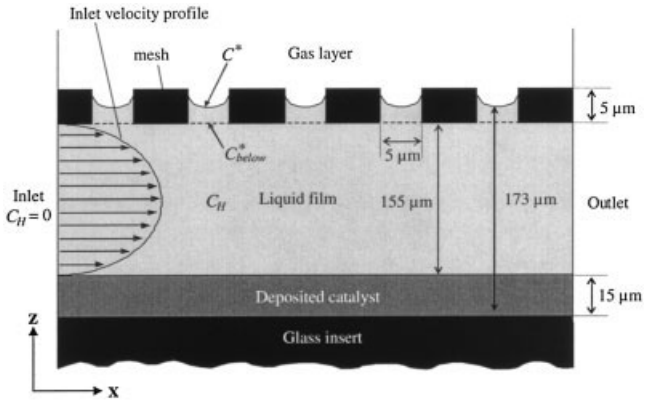

Figure 3. Computation domain in the plane x, z (reactor presentation, not at scale).

volume of solid catalyst is defined as $r(C_s)$ (mol.m^{-3}_{cata}.s^{-1}) = $a_c(C_s)\rho_p W_p$, where ρ_p and W_p are the solid density, and the Pd content of the solid catalytic layer, respectively.

Considering the hydrogen concentration range used in this study, as well as a likely strong external mass-transfer limitation, the denominator of Eq. 1 ranges between 1 and 1.9, the later values would result in a formal 0.73 reaction order with respect to hydrogen. For comparison, a first-order law with respect to hydrogen was also considered (Eq. 2)

$$a_c(\text{mol}\cdot g_{\text{Pd}}^{-1}\cdot s^{-1}) = k_0 \exp\left(-\frac{E_a}{RT}\right) K_H C_H \tag{2}$$

The Wilke-Chang correlation,[27] gives the molecular diffusivity (D_M) value at 298 K of $6.81\text{x}10^{-9}$ m^2s^{-1}, and 6.55×10^{-9} $m^2.s^{-1}$ in methylcyclohexane and α-methylstyrene, respectively. In the case of mixtures, the modified Wilke-Chang correlation gives $D_{M.} = 6.65 \times 10^{-9}$ $m^2.s^{-1}$. The influence of the temperature on D_M was estimated using the Tyn correlation. Because the tortuosity of γ-alumina ranges from 2 to 3, and the internal porosity is about 0.6, the effective diffusivity D_E is estimated as $D_M/4$.

The equilibrium hydrogen concentration is estimated using Eq. 3, which is adapted from the equation of Herskowitz to consider the higher pressure and the solvent composition[28]

$$C^*\ (\text{mol}\cdot m^{-3}) = (0.0145T - 1.6985) \times P\ (\text{bar}) \times 1.3 \tag{3}$$

This equation gives the equilibrium concentration C* in the liquid at the meniscus interface in the holes (Figure 3). The concentration just below the mesh is unknown and has been determined by Fluent® (from 2-D model), and taken as $C^*_{below} = C^*_{\text{Fluent}} = 0.96C^*$ in the case of a liquid film thickness of 155 μm.

Experimental data analysis

The method used for the determination of K_La is based on the measurement of the apparent rate of a fast chemical reaction of known intrinsic kinetics. The reaction is the hydrogenation of the α-methylstyrene (AMS) catalyzed by palladium on alumina.[29]

In order to compute the mass-transfer coefficient from the conversion numbers for the reaction $A + H_2 \rightarrow B$, the following traditional assumptions have been made:

- The gas reagent (H_2) is the limiting reagent.
- The catalyst is completely wetted by the liquid.
- The thickness of the solid layer L is constant and the metal loading on the γ-alumina support is homogeneous (W_{Pd} is constant).
- Mass-transfer resistance in the gas phase is negligible (that is, pure H_2)
- The heat transfer in the catalyst layer is not limiting ($\Delta T < 2°C$).
- The specific G-L interfacial area, and the liquid thickness are constant, thus, a constant volumetric mass-transfer coefficient K_la is considered over the all reactor.

Note that most of these assumptions have been either checked experimentally and/or supported by estimations.

Since the intrinsic rate is independent of C_A and considering a constant mass-transfer coefficient, a constant hydrogen surface concentration at the catalyst surface C_S is assumed. This hypothesis will be confirmed by the numerical simulations. Thus, the apparent rate $\bar{r}$ will only depend on the hydrogen concentration on the surface of the catalyst layer, the temperature, the diffusivity, and the thickness of the catalyst layer ($\bar{r} = f(C_S, T, D_E, L)$).

Considering the following boundary conditions at reactor inlet and outlet

$$\left.\begin{array}{l}\text{inlet: } F_A = F_A^i = C_A^i Q_L \\ \text{Outlet: } F_A = F_A^o = C_A^o Q_L\end{array}\right| \tag{4}$$

Integration of the steady-state plug flow reactor model (Eq. 5) gives the relation between the apparent rate of reaction and the operating conditions, and the measured conversion (Eq. 6)

$$-\bar{r} d\nu_{cata} = dF_A \tag{5}$$

$$\bar{r} = \frac{F_A^i - F_A^o}{V_{cata}} = \frac{\chi F_A^i}{V_{cata}} = \frac{\chi C_A^i Q_L}{V_{cata}} \tag{6}$$

To account for the mass-transfer resistances from the gas to the solid, and considering a laminar flow of the liquid phase, a purely diffusive model is chosen. Note that the laminar flow hypothesis is supported by the very low Reynolds numbers < 1.5 (see section "Comparison between the numerical and experimental results"). Thus, the continuity of the hydrogen flux from the gas layer to the catalyst is described by Eq. 7, where K_La is the overall gas-liquid-solid mass-transfer coefficient (with $a = 4\ a_{G\text{-}L} = a_S$)

$$K_L a(C^* - C_s)V_L = \eta_S a_c(C_s)\rho_p W_p V_{\text{cata}} = \eta_S r(C_s)V_{\text{cata}} = \bar{r}V_{\text{cata}} \tag{7}$$

The effectiveness factor η_s for a flat catalytic layer and the Thiele modulus for a first-order reaction is given in Eqs. 8 and 9, respectively

$$\eta_S = \frac{\tanh(\Phi)}{\Phi}; \tag{8}$$

$$\Phi^2 = \frac{a_c \rho_p W_p L^2}{D_E C_S} \tag{9}$$

The unknown parameters in the set of Eqs. 7, 8 and 9 are C_S, $K_L a$, η_s, Φ. It is solved for K_L a using the Excel® solver.

CFD Simulation

The global approach described in the last section assumes a mass-flux equilibrium between the gas and the liquid film, and the catalyst along the reactor, whatever the reactor design and the flow pattern (Eq 7). However, experimental data are required, that is, the conversion, in order to compute concentration profile and the mass-transfer coefficient. The advantage of the CFD approach is to introduce the reactor geometry and to avoid the mass-flux equilibrium assumption. Only assumptions about the physical properties of the species and about the kinetics of hydrogenation must be done. However, owing to the high-aspect ratio, that is. the reactor width over the reactor length, the design must be simplified. First, a 2-D approach is used to compute the mean concentration at the bottom of the mesh (see Figure 3). Then, a 3-D model is developed in order to compute the hydrogen concentration in the presence of the hydrogenation reaction localized in the catalyst layer. In the two cases, the simulations are performed with the commercial software FLUENT®.

3-D numerical model

The computation is simplified at different levels. The computational domain is considered as a 0.5° sector for the sake of computational time. Its radius and its depth are 3 cm and 170 μm, respectively. Therefore, the velocity field and the chemical species concentrations are assumed to be independent of the tangential angle. The liquid is assumed to be a thin film between the catalyst and the gas. The depths of the liquid film and of the deposited catalyst are 15 μm and 155 μm, respectively. The catalyst is considered as a homogeneous and isotropic porous medium. No roughness is assumed at the liquid/catalyst interface. The permeability is small enough to impose a null velocity in the catalyst. Therefore, in this region, the local chemical species concentration is controlled by the equilibrium between the effective diffusion process and the chemical reaction. Inside the liquid film, the radial velocity has a parabolic profile in the axial direction. In order to insure the mass conservation, the velocity averaged over the liquid depth must decrease as 1/×. The imposed flow rate is equal to 9.25×10^{-12} m^{-3}s^{-1}($1.67\times10^{-9}\times0.5°/90°$). The gas-liquid interface is assumed to be continuous and located at z = 170μm, that is, below the mesh. The mesh is, therefore, not taken into account in the computational domain. However, its presence in the reactor induces a mean hydrogen concentration C^*_{below} at z = 170μm less than the concentration at equilibrium. The value of C^*_{below}, estimated with the 2-D model described later, is 9.3 mol.m$_L^{-3}$. At the inlet (located at x = 1mm), the imposed concentration of α-methylstyrene, methylcyclohexane and hydrogen are respectively 3,300, 4,480 and 0 mol.m^{-3}. A periodic condition is imposed at the two opposite vertical planes of the sector (that is, in the tangential direction). The density, the viscosity of the liquid and also the molecular-diffusion coefficient of each species do not change with the composition of the mixture. The kinetic of the catalytic reaction, located in the catalyst, is defined as $a_c \rho_p W_{Pd}$. The chemical reaction depends on the hydrogen concentration only. Therefore, one may assume that the molecular diffusion, of all the species, is equal to that of hydrogen. The adopted meshing is structured. The numbers of hexahedral cells in the liquid film are 300 × 310 × 1 in radial, axial and tangential direction respectively. In the catalytic region, the cells numbers are 300 × 30 × 1. The QUICK scheme is used to solve the stationary mass transport equations.

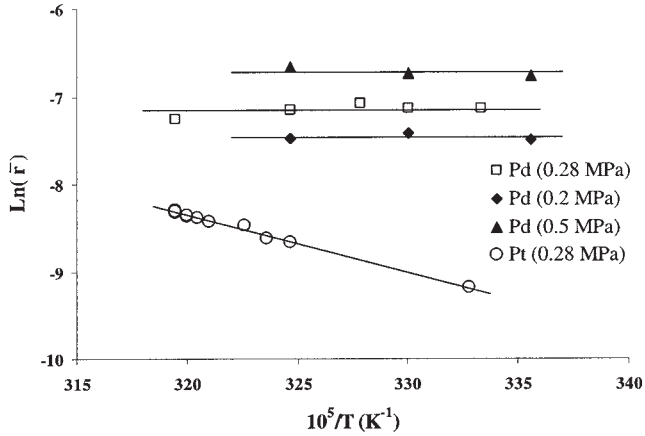

Figure 4. Arrhenius plot for the palladium and platinium catalysts.

2-D numerical model

As in the 3-D model, the same assumptions are used in the 2-D model. However, in order to compute the hydrogen concentration profile at the bottom of the mesh, the gas-liquid interface is modeled by a set of meniscus with a radius of 5 μm. The distance between two meniscuses is 20 μm. The bottom of each meniscus is arbitrary chosen at z = 158 μm. The length of the computational domain is 2.5 mm. The equilibrium hydrogen concentration (9.7 mol.m^{-3}) is imposed at the gas-liquid interface. A parabolic profile of the radial velocity is imposed at the inlet. The mean velocity over the liquid depth is constant and equal to 428 μms^{-1}, that is, the mean velocity in the 3-D model. The number of cells is 20 × 2,500 in the catalytic region and 200 × 2,500 in the liquid film. Owing to the small size of the meniscus, the mesh is refined in the region z > 150 μm.

Results and discussions

As can be seen in Figure 4, an activation energy (E_a) close to zero is obtained for the tests carried out under the different pressure conditions (P = 0.2, 0.28 and 0.5 MPa) with the fast palladium catalyst (1 %wt Pd/γ-Al_2O_3). This likely indicates a strong external mass-transfer limitation. The calculated surface concentration of hydrogen C_S is in the range 1.2 to 4.5 mol.m$_L^{-3}$, thus, below the equilibrium concentration of hydrogen at the gas-liquid interface C* (Table 1). Such a large

Table 1. Operating Conditions and Experimental Results for the Pd/γ-Alumina Catalyst[a]

Entry	Mode	P MPa	T K	Q_L 10^{-9} $m_L^3 \cdot s^{-1}$	χ %	C^* $mol \cdot m_L^{-3}$	C_s $mol \cdot m_L^{-3}$	η_S	K_La s^{-1}
1	Pulse	0.28	300	1.67	18	9.7	2.50	0.22	1.19
2	Pulse	0.28	303	1.67	20	9.8	2.50	0.21	1.28
3	Pulse	0.28	308	1.67	20	10.1	2.09	0.19	1.16
4	Pulse	0.28	313	1.67	18	10.7	1.59	0.17	0.91
5	Pulse	0.28	305	1.67	22	9.9	2.50	0.20	1.34
6	Pulse	0.2	298	1.67	14	6.8	2.03	0.23	1.38
7	Pulse	0.2	303	1.67	15	7.0	1.84	0.20	1.37
8	Pulse	0.2	308	1.67	15	7.2	1.48	0.18	1.17
9	Pulse	0.5	298	1.67	29	17.0	4.46	0.24	1.08
10	Pulse	0.5	303	1.67	30	17.5	3.89	0.22	1.03
11	Pulse	0.5	308	1.67	32	18.0	3.53	0.19	1.03
12	Pulse	0.2	298	1.67	20	6.8	2.90	0.23	2.34
13	Pulse	0.2	298	1.67	18	6.8	2.68	0.23	2.06
14	Pulse	0.2	298	1.67	21	6.8	3.09	0.23	2.61
15	Continuous	0.2	298	3.33	7	6.8	1.98	0.23	1.34
16	Continuous	0.2	298	1.67	11	6.8	1.53	0.22	0.96
17	Continuous	0.2	298	0.83	23	6.8	1.60	0.22	1.02
18	Continuous	0.2	298	0.42	37	6.8	1.27	0.22	0.77
19	Continuous	0.2	298	0.42	41	6.8	1.42	0.22	0.88
20	Continuous	0.2	298	1.67	10	6.8	1.38	0.22	0.85

[a]Estimated error for C_s, K_La, and η_S is ±20%.

difference between the two hydrogen concentrations also indicates a limitation by the external mass transfer. The results shown in Table 1 are calculated by considering the more complex rate law of Eq. 1. Similar calculation with the first-order rate law (Eq. 2) leads to only ca. 15–20 % difference. The low values of the effectiveness factor η_S (ca. 0.2) indicate that the reaction is also strongly limited by the intragranular diffusion. The mean value of the mass-transfer coefficient (K_La) computed from the experimental data is ca. 1.2 ± 0.4 s^{-1}. The kinetic law for the platinum catalyst for the same reaction is under investigation. However, the intrinsic activity from preliminary kinetic studies is roughly 7–10 times slower than the palladium catalyst. Using the Pt catalyst (0.9 wt %), the reactor likely operates in the chemical regime since an activation energy of 40 $kJ.mol^{-1}$ is obtained (Figure 4).

In the presence of a chemical reaction in the catalytic layer, the low porosity of the mesh makes the slope of the concentration profile along the mesh depth higher than along the liquid film one, so that C_{below} should be lower than the concentration at equilibrium despite the small distance between the minescus position and the lower mesh-side position. For example, the computation, carried out with a liquid film of 75μm depth and a catalytic one of 25μm, gives C_{below} = 0.85C*, and Cs = 0.103 C*, with a slop of.01C* and 05C* through the liquid film and through the mesh, respectively. Near the mesh, the concentration oscillates with an amplitude of 0.088C* and a periodicity corresponding to the pore location. This oscillation, developed by the nonuniform gas-liquid contact, is attenuated rapidly as z decreases and disappears when z is lower than 90μm. The concentration C_{below} decreases with the liquid layer depth : if the liquid film and the catalytic layer have a depth of 50 μm, the numerical computation gives C_{below} = 0.78 C*, and Cs = 0.137 C*. The actual geometry keeps the catalytic layer far from the mesh (155 μm), which leads to C_{below} close to C* (0.96 C*).

Figure 5 shows the axial profile of hydrogen concentration at different radial position in the case of the 3-D model. As mentioned previously, the concentration at the gas-liquid interface is the concentration just below the mesh in the 2-D model. The profiles at x = 1 cm and 3.1 cm are identical : the asymptotic one is reached after 5 mm. This higher distance compared to the 2-D model (1 mm) is explained by the 1/x dependence of the velocity in the 3-D mode,l which results in a higher mean velocity at the inlet of the 3-D model: at x = 1mm, the mean velocity is 0.68 $cm.s^{-1}$ for a mean velocity of 423 $\mu m.s^{-1}$ over all the liquid film volume. The asymptotic concentration at the catalyst/liquid interface is equal to that of the 2-D asymptotic model. This means that the concentration in the catalyst is sensitive only to the mean concentration at the mesh location. The concentration decreases linearly from the top to the bottom of the liquid film and exponentially in the catalyst which is active in a layer of 5 μm depth. The high decrease of the concentration means that the molecular diffusion is a limiting process. Qualitative comparisons of the

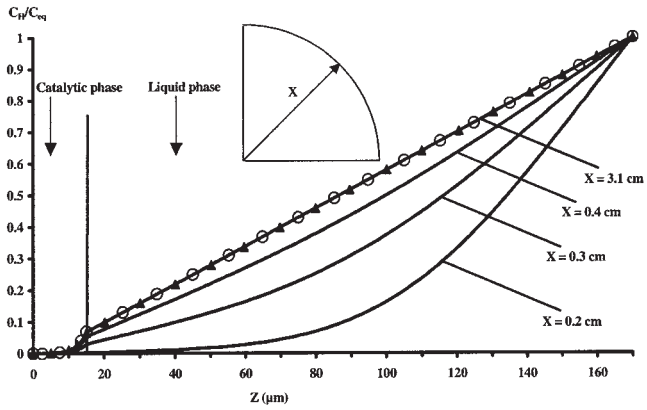

Figure 5. Axial profile of the normalized hydrogen concentration for the 3-D numerical simulations at different radial positions (lines), for the refined mesh simulations (▲), and for the analytical solution with a first-order reaction (—○—), and top view of the reactor.

Table 2. Parameter Sensitivity Analysis for the 3-D Model

		E_a (kJ · mol^{-1})		τ/β		D_M 10^{-9} (m^2 · s^{-1})		C^*_{below} (mol · m^{-3})	
	Reference[a]	41	36	2	8	3.32	13.3	7.0	12.43
χ (−)	0.045	0.041	0.05	0.047	0.044	0.024	0.085	0.035	0.006
$\langle C_H \rangle_{\text{cata}}$ (mol · m^{-3})	0.113	0.27	0.04	0.116	0.111	0.058	0.219	0.085	0.152
C_S (mol · m^{-3})	0.603	1.12	0.374	0.511	0.862	0.452	0.965	0.485	0.862

[a]Computed with the standard values: E_a = 38.7 kJ · mol^{-1}, τ/β = 4, D_M = 6.65 · 10^{-9} m^2 · s^{-1}, C^*_{below} = 9.3 mol · m^{-3} (see Table 1, entry 1, and section "Reactor description and experimental set-up").

characteristic diffusion time through the liquid film (taken as d_{liq}^2/D_M = 3.6 s) and through the catalyst layer (taken as L^2/D_E = 0.14 s), and of the characteristic time of the chemical reaction (taken from Eq. 2 as $1/[K_H k_O \rho_p W_{pd} \exp(-(E_a/RT))]$ = 0.00455 s) support the idea of strong diffusion limitations. The conversion, defined as $\chi = (1/C_A Q_L) \int_{Vcata} a_c(C_S) \rho_p W_{pd} dV$, is found to amount 4.5%. Note that for x < 1 cm, the asymptotic concentration profile is not reached, which would lead to a lower conversion in this section of the reactor. However, the corresponding volume is only 10% of the total reactor volume, thus, the contribution to the total conversion is negligible. This is supported by the good agreement between the numerical conversion (4.5%), and that obtained from the analytical model (5%) (see later), which consider a constant radial hydrogen concentration.

Comparison between the numerical and experimental results

Very different concentration at the catalyst surface (C_S(fluent) = 0.6 mol.m^{-3}, C_S(experiment) = 2.5 mol.m^{-3}) are obtained with the two methods (see Table 1 (Entry 1) and Table 2 (first column)). Consequently, a large difference in the conversion is calculated (χ(fluent) = 4.5%, χ (experiment) = 18.5 %). This low value of conversion compared to the experimental one is confirmed in two ways: by refining the mesh in the region 0 μm < z < 35 μm all along the radial direction, and by computing an analytical solution in the case of a linear kinetic (see Appendix A). Figure 5 shows that mesh refining has no effects on the results and the analytical solution gives similar results, and a conversion of 5% assuming that $C_{z=0}$ = 0 mol.m^{-3}.

The numerical results depend on several parameters (tortuosity, molecular diffusivity, concentration at the mesh, kinetic prefactor, and so on), the values of which are either averaged from the published literature (τ), adapted from published correlations (D_M), difficult to assess due to geometrical particularities of the mesh contactor (C*), or well determined albeit with a rather large confidence interval (Ea). Thus, a parameter sensitivity study has been carried out with different values as shown in Table 2. In each simulation, one of the values is modified in order to identify the parameter to which the 3-D model is most sensitive. The modified value is displayed in the first row of Table 2. The simulations show that the four variables (χ, $<C_H>_{\text{cata}}$, C_S, $K_l a$) depend mostly on the diffusion process in the liquid film via the molecular diffusion, as they are not sensitive to the tortuosity. This confirms the observation made earlier, but cannot account for the much higher measured conversion.

Finally, the influence of the thickness of the liquid layer d_{liq}, was evaluated. Indeed, a decrease of d_{liq} would result in a more efficient hydrogen transfer from the gas phase to the liquid phase. Thus, the set of Eqs. 7, 8 and 9 was solved for d_{liq} instead of $K_L a$. That was achieve by considering the following definitions of K_L and Eq 10, and solving Eq. 11.

$$K_L \text{ (m} \cdot \text{s}^{-1}) = \frac{D_M}{d_{liq}} \text{ and } a \text{ (m}^2 \cdot \text{m}_L^{-3}) = \frac{S}{V_L} = \frac{1}{d_{liq}} \quad (10)$$

$$K_L a (C^* - C_s) V_L = \frac{D_M}{d_{liq}} S (C^* - C_s) = \eta_S a_c(C_s) \rho_p W_p V_{\text{cata}} = \bar{r} V_{\text{cata}} \quad (11)$$

Numerical values of d_{liq} in the range 75 to 100 μm are obtained, that is, much shorter than the geometrical thickness of 155 μm. Figure 6 presents a parity plot between the experimental and calculated conversion using liquid-layer thickness of 155 μm and 90 μm. A similar parity plot is obtained with the pulse experiments. The experimental data are well in line with the later thickness. Such a shorter distance quantitavely explains the increase of the transport process in the liquid film during the experiments, and the higher observed conversions. Such a shrinking of d_{liq} is explained by the presence of a gas

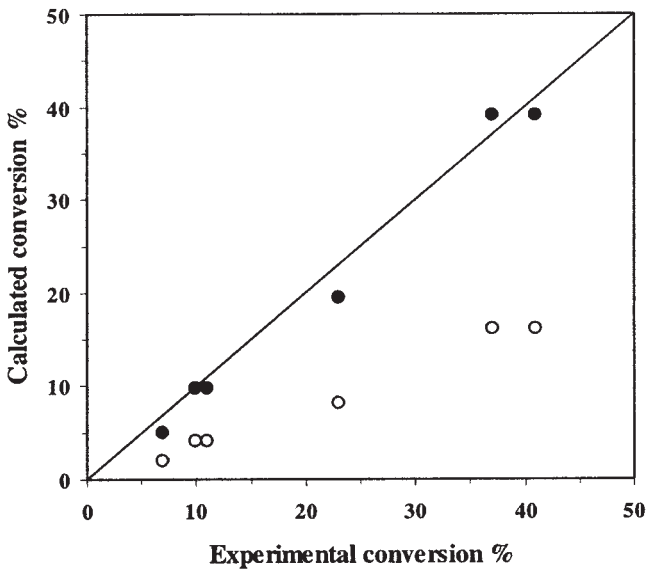

Figure 6. Experimental and calculated conversion for the continuous flow experiments with: $K_L a = D_M/d_{liq}^2$: d_{liq} = 155 μM (○) and d_{liq} = 90 μm (●).

bubble located just below the mesh and stabilized by the mesh. This hypothesis is under current investigation. Note that shorter d_{liq} (ca. 90 μm) obviously translate into higher computed K_La values (ca. 1 s^{-1}) in agreement with the experimental K_La depicted in Table 1.

Conclusions

The global gas-liquid-solid mass-transfer coefficient in the mesh microreactor has been determined by a chemical method and compared to CFD simulations, as well as to a more traditional analytical method. The CFD–2-D model gives the equilibrium hydrogen concentration below the mesh, a value that is not available experimentally. The 3-D model gives the hydrogen concentration profile in the liquid and in the catalyst films. The experimental K_La value of ca. 1 s^{-1} is well above that predicted by the film theory (0.3 s^{-1}). This is explained by a shrinking of the liquid layer thickness to ca. 90 μm likely caused by a stable and reproducible entrapped gas bubble.

Currently, experimental conversions are higher than that predicted with the geometrical liquid layer thickness of 155 μm. Compared to traditional laboratory 3-phase reactors (fix beds, tank reactors, bubble columns, and so on) the mesh contactor offers interesting properties, such as better control of the flow, of the gas-liquid and liquid-solid contact, faster startup and shutdown, and safer operations under pressure due to lower reagents inventory. Furthermore, with respect to fix-beds reactors, it displays a much better mass-transfer efficiency. Many studies concerning intrinsic kinetics, catalyst deactivation, screening of catalysts/substrates for reactions involving liquid-liquid, gas-liquid or gas-liquid-solid mixtures that are either fast and/or exothermic, or involve toxic or expensive reagents are foreseen with this tools. Screening and kinetic applications in multiphase catalysis (gas-liquid, gas-liquid-solid, and liquid/liquid) are currently performed with this setup and will be published soon. CFD results encourage future uses of modeling for the estimation of mass and heat-transfer performances, but also to help equipment selection, design and characterization. Future works are ongoing to design microstructured gas-liquid contactors, also based on film separation using capillary forces at the micrometer scale (5 μm), but with controlled thinner liquid layer to provide a higher mass-transfer capability.

Acknowledgment

This research was supported by the European Commissions through the KEMICC project (GRD-2000-256262). Dr. John Shaw and David Wenn are warmly acknowledged for the fabrication of the mesh-contactor. Many thanks to Prof. Julian Ross and Dr. Serguei Belochapkine from Limerick University for the alumina washcoat deposition.

Notation

$a_{G\text{-}L}$ = gas-liquid interfacial area per liquid phase volume, $m^2.m_L^{-3}$
a_S = liquid-solid interfacial area per liquid phase volume, $m^2.m_L^{-3}$
$a_c(C_s)$ = intrinsic activity, $mol.g_{Pd}^{-1}.s^{-1}$
AMS = α-methylstyrene
C_A = concentration of α-methylstyrene at the reactor inlet, $mol.m_L^{-3}$
C_0 = hydrogen concentration at z = 0 μm, $mol.m_L^{-3}$
C^* = hydrogen concentration at equilibrium, $mol.m_L^{-3}$
C_H = hydrogen concentration dissolved in the liquid, $mol.m_L^{-3}$
C_S = hydrogen concentration at the catalyst surface (z = 15 μm), $mol.m_L^{-3}$
C^*_{below} = hydrogen concentration at equilibrium below the mesh computed with Fluent, $mol.m_L^{-3}$
$<C_H>_{cata}$ = mean hydrogen concentration in the catalytic layer, $mol.m^{-3}$
d_{liq} = liquid film thickness, m
D_M = hydrogen molecular diffusion coefficient, $m^2.s^{-1}$
D_E = hydrogen effective diffusion coefficient in the catalyst, $m^2.s^{-1}$
Ea = activation energy, $J.mol^{-1}$
F_A = molar flow rate, $mol.s^{-1}$
k_0 = arrhenius pre-exponential factor, $mol.s^{-1}.g_{Pd}^{-1}$
K_H = adsorption equilibrium constant of hydrogen, $m_L^3.mol^{-1}$
k' = Rate constant at 279 K, $mol.s^{-1}.g_{Pd}^{-1}$
K_La = global gas-liquid-solid mass-transfer coefficient, s^{-1}
L = catalytic layer thickness, m
P = pressure, MPa
Q_L = volumetric liquid flow rate, $m_L^3.s^{-1}$
$r = r(C_s)$ = Intrinsic reaction rate, $mol.m_{cata}^{-3}.s^{-1}$
$\bar{r}$ = Apparent rate, $mol.m_{cata}^{-3}.s^{-1}$
R = universal gas constant, $J.mol^{-1}.K^{-1}$
S = geometrical surface of the cavities, m^2
T = temperature, K
V_{cata} = volume of the catalytic layer, m_{cata}^3
V_L = volume of the liquid film, m_L^3
W_{Pd} = Pd content of the solid catalytic layer, wt%
x = radial coordinate, m
z = axial coordinate, m

Greek letters

β = porosity of γ-alumina
ε_S = solid holdup, $m_{cata}^3.m_{L+cata}^{-3}$
η_S = effectiveness factor, dimensionless
Φ = thiele modulus, dimensionless
ρ_p = dry particle density, $g_{cata}.m_{cata}^{-3}$
τ = tortuosity, dimensionless
χ = conversion, %

Subscripts and superscripts

A = α-methylstyrene
i = inlet
o = outlet

Literature Cited

1. Hessel V, Hardt S, Löwe H. *Chemical Micro Process Engineering (Fundamentals, Modelling and reactions)*. New York: Wiley-VCH; 2004.
2. Hessel V, Löwe H, Müller A, Kolb G. *Micro Chemical Process Engineering (Processing and Plants)*. New York: Wiley-VCH; 2005.
3. Jähnisch K, Hessel V, Löwe H, Baerns M. Chemistry in microstructured reactors. *Angew Chem Int Ed*. 2004;43:406.
4. Abdallah R, Meille V, Shaw J, Wenn D, de Bellefon C. Gas-liquid and gas-liquid-solid catalysis in a mesh microreactor. *Chem Commun*. 2004;372.
5. Abdallah R, Ireland T, de Bellefon C. Discovering new water-soluble catalysts for the liquid-liquid isomerization of allylic alcohols using microdevices. *Chem Ing Tech*. 2004;76:633.
6. de Bellefon C, Pestre N, Lamouille T, Grenouillet P, Hessel V. High throughput kinetic investigations of asymmetric hydrogenations with microdevices. *Adv Synth & Catal*. 2003;345:190.
7. Schönfeld F, Hardt S. Simulation of helical flows in microchannels. *AIChE J*. 2004;50:771.
8. Yamaguchi Y, Takagi F, Yamashita K, Nakamura H, Maeda H, Sotowa K, Kusakabe K, Yamasaki Y, Morooka S. 3-D simulation and visualization of laminar flow in a microchannel with hair-pin curves. *AIChE J*. 2004;**50:**1530.
9. Heibel AK, Lebens PJM, Middelhof JW, Kapteijn F, Moulijn J. Liquid residence time distribution in the film flow monolith reactor. *AIChE J*. 2005;51:122.

10. Bhattacharya M, Harold MP, Balakotaiah V. Mass-transfer coefficient in washcoated monoliths. *AIChE J*. 2004;50:2939.
11. van Baten JM, Krishna R. CFD simulations of mass transfer from Taylor bubbles rising in circular capillaries. Chem. Eng. Sci. 2004;59**:** 2535.
12. Angeli P, Gobby D, Gavriilidis A. Modelling of gas-liquid catalytic reactions in microchannels. In: Wolfgang E. *Microreaction Technology: Industrial Prospects*. Berlin: Springer-Verlag; 1999:253.
13. Klöker M, Kenig EY, Piechota R, Burghof S, Egorov Y. CFD-based study on hydrodynamics and mass transfer in fixed catalyst beds. *Chem Eng Tech*. 2005;28:31.
14. Pollack MG, Fairb RB, Shenderov AD. Electrowetting-based actuation of liquid droplets for microfluidic applications. *Appl Phys Let*. 2000; 77:1725.
15. Jähnisch K, Baerns M, Hessel V, Ehrfeld W, Haverkamp V, Lowe H, Wille Ch, Guber A. Direct fluorination of toluene using elemental fluorine in gas-liquid microreactors. *J Fluorine Chem*. 2000;105:117.
16. de Mas N, Günther A, Schmidt MA, Jensen KF. Microfabricated multiphase reactors for the selective direct fluoration of aromatics. *Ind Eng Chem Res*. 2003;42:698.
17. Doku GN, Verboom W, Reinhoudt DN, van den Berg A. Microbubble beam (MBB), a potential dispersion mechanism for multiphase gas-liquid microreactor systems. *Ind Eng Chem Res*. 2003;42:3721.
18. Yeong KK, Gavriilidis A, Zapf R, Hessel V. Experimental studies of nitrobenzene hydrogenation in a microstructured falling film reactor. *Chem Eng Sci*. 2004;59:3491.
19. Zanfir M, Gavriilidis A, Wille Ch, Hessel V. Carbone dioxide absorption in a falling film microstructured reactor :experiments and modelling. *Ind Eng Chem Res*. 2005;44:1742.
20. Wenn D, Shaw J, Mackenzie B. A mesh microcontactor for 2-phase reactions. *Lab on a Chip*. 2003;3:180.
21. Chambers RD, Helling D, Spink RCH, Sandford G. Gas-liquid thin film for selective direct fluorination. *Lab on a Chip*. 2001;1:132.
22. Chambers RD, Helling D, Ress AJ, Sandford G. Microreators for oxidations using fluorine. *J Fluorine Chem*. 2003;119:81.
23. Losey MW, Schmidt MA, Jensen KF. Microfabricated multiphase packed-bed reactors: characterization of mass transfer and reactions. *Ind Eng Chem Res*. 2001;40:2555.
24. Pennemann H, Watts P, Haswell S, Hessel V. Benchmarking of microreactor applications. *Organ Proc Res Dev*. 2004;8:422.
25. Ehrfeld W, Hessel V, Löwe H. Microreactors: *New technology for modern chemistry*. New York: Wiley-VCH; 2000.
26. Meille V, de Bellefon C, Schweich D. Kinetics of α-Methylstyrene Hydrogenation on Pd/Al_2O_3. *Ind EngChem Res*. 2002;41:1711.
27. Reid R, Prausnitz J, Polling B. *The Properties of Gases & Liquids*. 4th ed. New York: McGraw-Hill Inc;1987.
28. Herskowitz M, Morita S, Smith J. Solubility of Hydrogen in α-Methylstyrene. *J Chem Eng Data.* 1978;23:227.
29. Meille V, Pestre N, Fongarland P, de Bellefon C. Gas-liquid mass transfer in small laboratory batch reactors: Comparison of methods. *Ind EngChem Res*. 2004;43:924.

Appendix A

Analytical expression of the hydrogen concentration in the case of a first-order kinetic

The medium is assumed to be infinitely long. Far from the inlet, the hydrogen concentration reaches the asymptotic profile depending on z only. Therefore, neglecting the transient region near the inlet, the transport of hydrogen into the catalyst can be written in the case of a first-order kinetic as

$$D_E \frac{\partial^2 C_H(z)}{\partial z^2} = -K' C_H(z) \text{ with } K' = K_o \rho_p W_{pd} \exp\left(-\frac{E_a}{RT}\right) K_H \tag{A1}$$

The concentration flux through the liquid film is equal to the chemical flux averaged over the catalyst depth

$$D_M \frac{C^*_{below} - C_s}{d_{liq}} = K' \int_0^L C_H(z) dz \tag{A2}$$

The concentration inside the catalyst has the following expression depending on the concentration at z = 0 μm

$$C_H = (C_S - C_0) \frac{Ch(\alpha z) - 1}{Ch(\alpha L) - 1} + C_0 \tag{A3}$$

where:

$$C_S = \frac{\frac{D_M C^*_{below}}{d_{liq} - L} - K' C_0 (A - L)}{\frac{D_M}{d_{liq} - L} + K' A} \tag{A4}$$

with

$$A = \frac{Sh(\alpha L)/\alpha - L}{Ch(\alpha L) - 1} \text{ and } \alpha = \sqrt{\frac{K'}{D_E}}$$

The conversion has the following expression $\chi = (1/C_A Q_L) \int_{Vcata} K' C_H dV$, and using relation Eq. A3, its expression becomes

$$\chi = \frac{K' V_{cata}}{F_A} \left[(C_S - C_0) \frac{Sh(\alpha L)/\alpha - L}{Ch(\alpha L) - 1} + C_0 L \right] \tag{5}$$

The mass-transfer coefficient is defined as $K_L a (C^*_{below} - C_S) V_L = K' \langle C_H \rangle_{cata} V_{cata}$. With the definition $\langle C_H \rangle_{cata} = (1/L) \int_0^L C_H(z) dz$, relation Eq. A2 gives

$$K_L a = \frac{D_M}{d^2_{liq}} \tag{6}$$

Manuscript received Jun 30, 2005, and revision received Jan. 31, 2006.